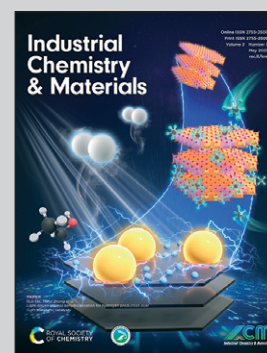**Showcasing research from Feng Yu's laboratory, School of Chemistry and Chemical Engineering, Shihezi University, Shihezi, China.**

A facile route of Ti decoration for modulating M–O–Ti (M = Ni, Co) and oxygen vacancies on NiCo-LDH electrocatalysts for efficient oxygen evolution reaction

Compared with NiCo-LDH, the as-obtained Ti-doped NiCo-LDH with abundant M–O–Ti (M = Ni, Co) bonds and oxygen vacancies exhibits excellent oxygen evolution reaction performance and water splitting activity.

Image reproduced by permission of Feng Yu from *Ind. Chem. Mater.*, 2025, **3**, 342.

As featured in:

See Xiaodong Yang,
Aiqun Kong, Feng Yu *et al.*,
Ind. Chem. Mater., 2025, **3**, 342.

ROYAL SOCIETY
OF **CHEMISTRY**

ICM
Industrial Chemistry & Materials

ROYAL SOCIETY OF CHEMISTRY

PAPER

Check for updates

A facile route of Ti decoration for modulating M–O–Ti (M = Ni, Co) and oxygen vacancies on NiCo-LDH electrocatalysts for efficient oxygen evolution reaction

Jing Xie,[a] Jianhao Du,[a] Pei Chen,[a] Gang Wang, [ID][a] Jinli Zhang, [ID][b] Xiaodong Yang, [ID] *[a] Aiqun Kong*[a] and Feng Yu [ID] *[ac]

Bimetallic layered double hydroxides (LDHs) have attracted substantial attention as oxygen evolution reaction (OER) catalysts. In this work, we provide a facile route to prepare Ti-doped NiCo-LDH/NF electrocatalysts with M–O–Ti (M = Ni, Co) covalent bonds *via* a rapid immersion method for the OER process. The experiments and density functional theory (DFT) calculations elucidate that the doping of Ti (M–O–Ti) not only exfoliates the NiCo-LDH nanosheets into spheres but also causes lattice distortion to produce more oxygen vacancies, which promotes faster exchange of intermediates and improves the electron transfer efficiency. These superior physical characters endow Ti-NiCo-LDH with an excellent overpotential of 319 mV at a current density of 50 mA cm^{-2}, which is markedly lower than that of NiCo-LDH (391 mV at 50 mA cm^{-2}). Even at a high current density of 100 mA cm^{-2}, NiCo-LDH displays an overpotential of 429 mV, whereas Ti-NiCo-LDH is capable of achieving an overpotential of 353 mV. Moreover, the water electrolyzer based on the Ti-NiCo-LDH bifunctional catalyst requires a low cell voltage of 1.60 V to achieve a current density of 10 mA cm^{-2}, and the Ti-NiCo-LDH catalyst has been successfully applied for solar cell-driven water electrolysis and the corresponding voltage is about 1.61 V. This work offers a novel strategy to fabricate high activity NiCo-LDH with rich oxygen vacancies toward the OER process.

1 Introduction

Green hydrogen produced by electrochemical water splitting is considered as a promising alternative to fossil fuels due to its renewability, high energy density (120 MJ kg^{-1}) and environmental friendliness.[1–3] However, the development bottleneck of water electrolysis is caused due to the slow-kinetics of the oxygen evolution reaction (OER) involving four-electron transfer processes.[4–6] Nevertheless, Ir/Ru-based catalysts have been employed as effective electrocatalysts for the OER process. As is well known, the high cost and scarcity of Ir/Ru-based catalysts severely hinder their use in commercial scale applications.[7–10] Therefore, it is urgent to develop low-cost, highly efficient and long-term stable non-precious metal catalysts for the alkaline OER.

Recently, transition metal hydroxides, especially two-dimensional transition metal layered double hydroxides (LDHs), have been rapidly developed due to their two-dimensional order and easily tailored structures.[11–15] In terms of OER activity, bimetallic NiFe LDH is considered to be one of the most efficient OER catalysts in alkaline solution.[16,17] However, the catalytic activity and stability deteriorate gradually over time due to the severe dissolution of iron in NiFe LDH and the long-term redox reaction.[18,19] Based on the above issues, the exploration of Fe-free LDH catalysts with high activity and outstanding stability is necessary. Accordingly, NiCo-LDH catalysts are expected to be potential alternative catalysts with superior OER performance.[20]

In order to expand the practical application of NiCo-LDH catalysts under high current densities, the catalytic activity of NiCo-LDH needs to be further improved. To solve the problems of poor intrinsic conductivity and agglomeration of layered structures and thus improve the electrochemical performance of LDHs, defect engineering is an efficient strategy to improve

[a] Key Laboratory for Green Processing of Chemical Engineering of Xinjiang Bingtuan, School of Chemistry and Chemical Engineering, Shihezi University, Shihezi 832003, China. E-mail: yangxiaodong1209@hotmail.com, kongaiqun@shzu.edu.cn, yufeng05@mail.ipc.ac.cn

[b] School of Chemical Engineering and Technology, Tianjin University, Tianjin 300072, P. R. China

*[c] College of Sciences, Shihezi University, Shihezi 832003, China*

electrocatalytic performance by intentionally introducing defects on the surface or inside the lattice of catalysts.[21] For example, Wang *et al.*[22] performed acid etching to create defects on CoFe LDH by adding a small amount of nitric acid to the CoFe LDH suspension. The acid etched LDHs exhibited better oxygen evolution performance than the pristine LDHs under alkaline conditions with a small Tafel slope and good durability. Fu *et al.*[23] proposed an elaborate atmosphere corrosion strategy to construct porous NiFe-LDH with rich edge/surface-Fe defects on Ni foam (NF). The nickel foam was first pre-treated with $FeCl_3$ solution and then placed in a sealed container with nitric acid vapor and air. O_2 and nitric acid vapor etched the sample, leading to the formation of irregular porous structures and abundant defects. Benefiting from the

abundant and fantastic edge/surface-Fe defects, the material exhibited excellent pro-catalytic activity. However, due to the extra anions such as NO_3^- needed to be induced and acid etching requiring precise control of the amount of acid used, the synthesis of LDHs is complex. Otherwise, it may lead to the collapse of the LDH structure. The requirements, along with the essential demands to achieve enhanced conductivity, increased active sites, and an optimized electronic structure, lead scientists towards a simple and viable strategy to prepare defect-rich NiCo-LDH, thereby improving catalytic activity toward OER performance.

Herein, we propose a facile and fast method for preparing Ti-NiCo-LDH/NF electrocatalysts with rich oxygen vacancies *via* a facile liquid phase impregnation process of NiCo-LDH/
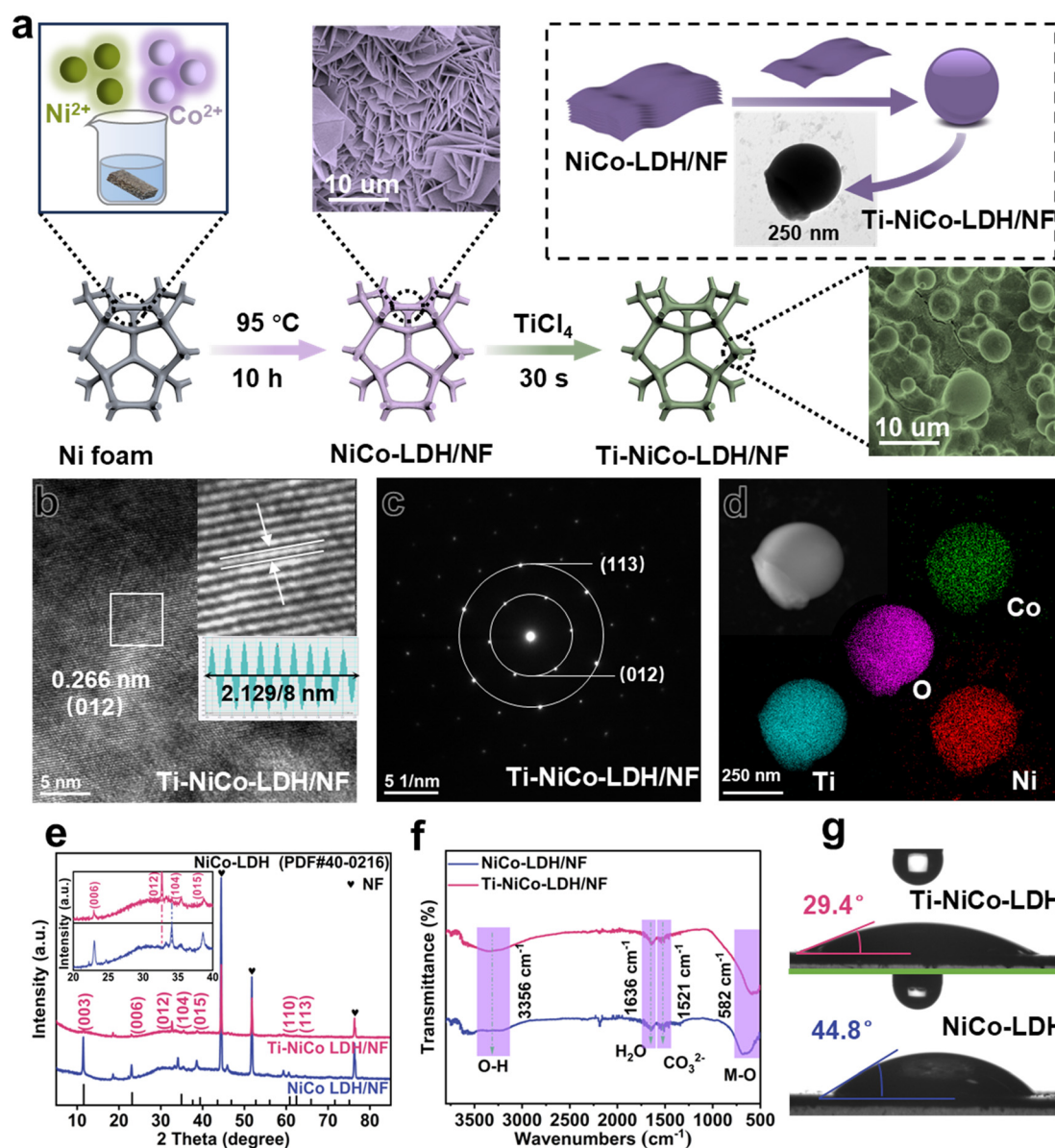
Fig. 1 (a) Schematic diagram of the process of exfoliating NiCo-LDH/NF nanosheets with $TiCl_4$; (b) HRTEM image of Ti-NiCo-LDH/NF; (c) SAED pattern of Ti-NiCo-LDH/NF; (d) energetic elemental mapping of Ni, Co, Ti, and O; (e) XRD spectra; (f) FTIR spectra of Ni-LDH/NF and Ti-NiCo-LDH/NF; (g) contact angles of Ni-LDH/NF and Ti-NiCo-LDH/NF.
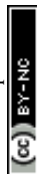
NF with titanium tetrachloride for 30 s. Specifically, Ti-doping induces the generation of oxygen vacancies, resulting in the improvement of intrinsic conductivity and the interfacial charge distribution, thereby remarkably promoting the OER catalytic activity intrinsically. Consequently, the optimized Ti-NiCo-LDH/NF electrode exhibits superior OER activity in alkaline aqueous solution, with overpotentials of 319 and 353 mV at current densities of 50 and 100 mA cm^{-2}, respectively. Also, the stability of the Ti-NiCo-LDH/NF electrode is also worth being highlighted. Moreover, the experiment result and density functional theory (DFT) calculations corroborate that the reaction of NiCo-LDH with TiCl$_4$ leads to the partial substitution of Ti for H atoms in M–O–H, forming abundant M–O–Ti (M = Ni, Co) covalent bonds. The formation of M–O–Ti (M = Ni, Co) covalent bonds efficiently regulates the electronic structure of Ni, facilitating the adsorption and resolution of the reaction intermediates, lowering the energy needed for RDS, which in turn enhances the catalytic activity of the OER. This work provides a new strategy for rapid modification of self-supported layered double hydroxides to achieve titanium doping to enhance OER catalytic activity.

2 Results and discussion

2.1 Structure and morphology of catalysts

The preparation procedures of Ti-NiCo-LDH/NF are illustrated in Fig. 1a. First, the precursors NiCo-LDHs were prepared by simple heating in a water bath at 95 °C for 10 h. After the hydrothermal reaction, NiCo-LDH nanosheets vertically aligned were obviously tightly covered on the NF skeleton surface (inset of Fig. 1a). After that, the obtained NiCo-LDH nanosheets were immersed into titanium tetrachloride solution for 30 s, and gradually evolved into NiCo-LDH nanospheres, indicating that Ti species and NiCo-LDH reacted and formed Ti-NiCo-LDH/NF. The main formation mechanism may be that the reaction of NiCo-LDH/NF with TiCl$_4$ caused Ti to partially replace the H atoms in M–O–H. Notably, the detailed microstructure and composition of Ti-NiCo-LDH were analysed by high resolution transmission electron microscopy (HRTEM). As shown in Fig. 1b, the lattice fringe spacing with a width of 0.266 nm was observed, which was ascribed to the (012) crystal plane of NiCo-LDH (PDF #40-0216).[24] Furthermore, the corresponding lattice spacing was slightly larger than the (012) lattice spacing of NiCo-LDH/NF (0.261 nm). We calculated the (012) interplanar spacing (d-spacing) of Ti-NiCo-LDH/NF using the XRD peak at 2θ = 32.67° (via Bragg's law: $d = \lambda/(2\sin\theta)$), yielding a value of 0.273 nm. Compared to undoped NiCo-LDH/NF (0.261 nm), the lattice spacing had expanded. This was consistent with the trend derived from TEM, which further demonstrated the interaction between NiCo-LDH/NF and TiCl$_4$. Since the atomic radius of titanium was much larger than that of hydrogen atoms, it may cause lattice distortion and increase the lattice spacing.[25] Meanwhile, the (012) and (113) diffraction rings of Ti-NiCo-LDH were visible on the selected area electron diffraction (SAED) mapping (Fig. 1c). The uniform distribution of Ni, Co, Ti, and O elements was reflected in the elemental mapping diagram (Fig. 1d), and ICP-OES measurement was performed in order to quantify the particular amount of Ni, Fe, and Si in these samples (Table 1), demonstrating the successful Ce doping indicating that titanium species were successfully doped into NiCo-LDH/NF.

The crystal structures and phase composition of Ti-NiCo-LDH/NF were further evaluated by X-ray diffraction (XRD). As shown in Fig. 1e, the prominent diffraction peaks at 11.51°, 22.94°, 32.67°, and 39.70° corresponding to the (003), (006), (012), and (015) planes of Ti-NiCo-LDH/NF were detected, which were in good agreement with literature reports.[26] A trace amount of nickel hydroxide impurities were generated in both catalysts. Although the diffraction peaks of Ti-NiCo-LDH/NF showed almost the same pattern without new characteristic peaks, the intensity of the diffraction peaks was significantly weaker compared to NiCo-LDH/NF, especially the (110) and (113) diffraction peaks that were almost absent. In addition, the diffraction peak of the (012) lattice plane for Ti-NiCo-LDH/NF was shifted towards lower angles, indicating the corresponding interplanar spacing expansion, which was beneficial to the improvement of the OER catalytic performance.[27] To identify the interlaminar anions of all LDH samples, FT-IR spectra were collected in the wavenumber range of 500–4000 cm^{-1}. As could be seen from Fig. 1f, a broad and strong absorption band located at 3356 cm^{-1} was observed for both samples, which was attributed to the stretching vibrations of the hydroxyl groups of the surface and interlayer water molecules in the LDH layer. The absorption peaks at 1636, 1521 and 582 cm^{-1} were assigned to the vibrational peaks of the water molecule, CO$_3^{2-}$ and M–O bond, respectively. The presence of carbonate ions in hydrotalcite was due to the absence of inert gas protection during the synthesis of hydrotalcite.[28] To further study the surface wetting ability of the catalysts, the water contact angles of NiCo-LDH/NF and Ti-NiCo-LDH/NF electrodes were separately tested. In Fig. 1g, the contact angle of Ti-NiCo-LDH/NF was 29.4°, which indicated it is more hydrophilic than NiCo-LDH/NF (44.8°), suggesting that the Ti-doping significantly changed the hydrophilicity of NiCo-LDH/NF. The more hydrophilic nature would effectively enhance the surface interactions between ions and active sites, thus promoting the adsorption kinetics of surface substances at the interface between the Ti-NiCo-LDH/NF electrode and electrolyte.[29,30]

To understand the surface composition and chemical state of the catalyst, X-ray photoelectron spectroscopy (XPS) was performed. For Ti-NiCo-LDH/NF, Ni 2p showed two

Table 1 The different metal contents in samples tested by ICP

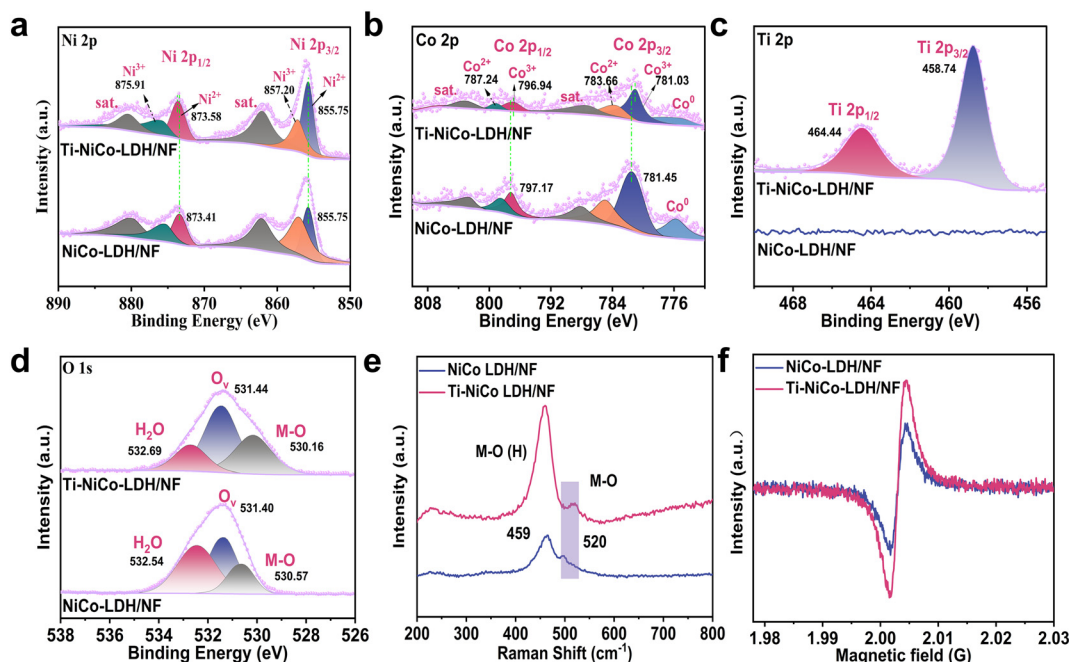| Sample	Ni	Co	Ti
NiCo-LDH/NF	94.7%	5.3%	0
Ti-NiCo-LDH/NF	93.2%	3.0%	3.4%

Fig. 2 Chemical states and electronic structural characterization of NiCo-LDH/NF and Ti-NiCo-LDH/NF. High-resolution XPS spectra of (a) Ni 2p, (b) Co 2p, (c) Ti 3d, and (d) O 1s; (e) Raman spectra; (f) EPR spectra.

characteristic peaks at 873.58 (Ni $2p_{1/2}$) and 855.75 eV (Ni $2p_{3/2}$), which corresponded to Ni^{2+}, respectively (Fig. 2a).[31–33] Moreover, the binding energy of Ni $2p_{1/2}$ in Ti-NiCo-LDH/NF was slightly higher than that in NiCo-LDH/NF. For the Co 2p spectrum, the peaks located at 775.65 eV and 775.39 eV were observed for both NiCo-LDH/NF and Ti-NiCo-LDH/NF, respectively, which belonged to metal Co (Co^0).[34,35] As shown in Fig. 2b, the high-resolution XPS spectrum of Co 2p showed two peaks of Co^{3+} at 796.94 and 781.03 eV, which were associated with Co $2p_{1/2}$ and Co $2p_{3/2}$, respectively.[36] In addition, the peaks at 787.24 and 783.66 eV were attributed to Co $2p_{1/2}$ and Co $2p_{3/2}$ of Co^{2+}, indicating the coexistence of Co^{2+} and Co^{3+}. Noticeably, the Co $2p_{1/2}$ and Co $2p_{3/2}$ of Co^{2+} in Ti-NiCo-LDH/NF shifted to a low energy level, suggesting that the doping of titanium (Ti) resulted in a partial electron transfer from Ni to Co and strong interfacial electronic interactions.[37] It was noteworthy that Ti 2p peaks in Ti-NiCo-LDH/NF appeared after doping of Ti species. In Fig. 2c, the Ti 2p spectrum showed two characteristic peaks located at 458.74 and 464.44 eV, which belonged to Ti–O coordination.[2,38]

Three distinct peaks at 530.16, 531.44, and 532.69 eV were observed in the O 1s spectra, which corresponded to the metal–oxide bond (M–O), oxygen vacancies (O_V), and absorbed water, respectively.[39] Obviously, the peak area ratio of O_V in Ti-NiCo-LDH/NF was larger than that in NiCo-LDH/NF, demonstrating that the incorporation of Ti effectively increased the concentration of O_V in Ti-NiCo-LDH/NF. Additionally, it was discovered that the Ti-doping caused a significant change in the electronic structure of O 1s, moving it to higher binding energies. Notably, Ti-NiCo-LDH/NF showed a higher lattice oxygen content (33.4%) than NiCo-LDH/NF (17.6%), which, together with the generation of Ti–O
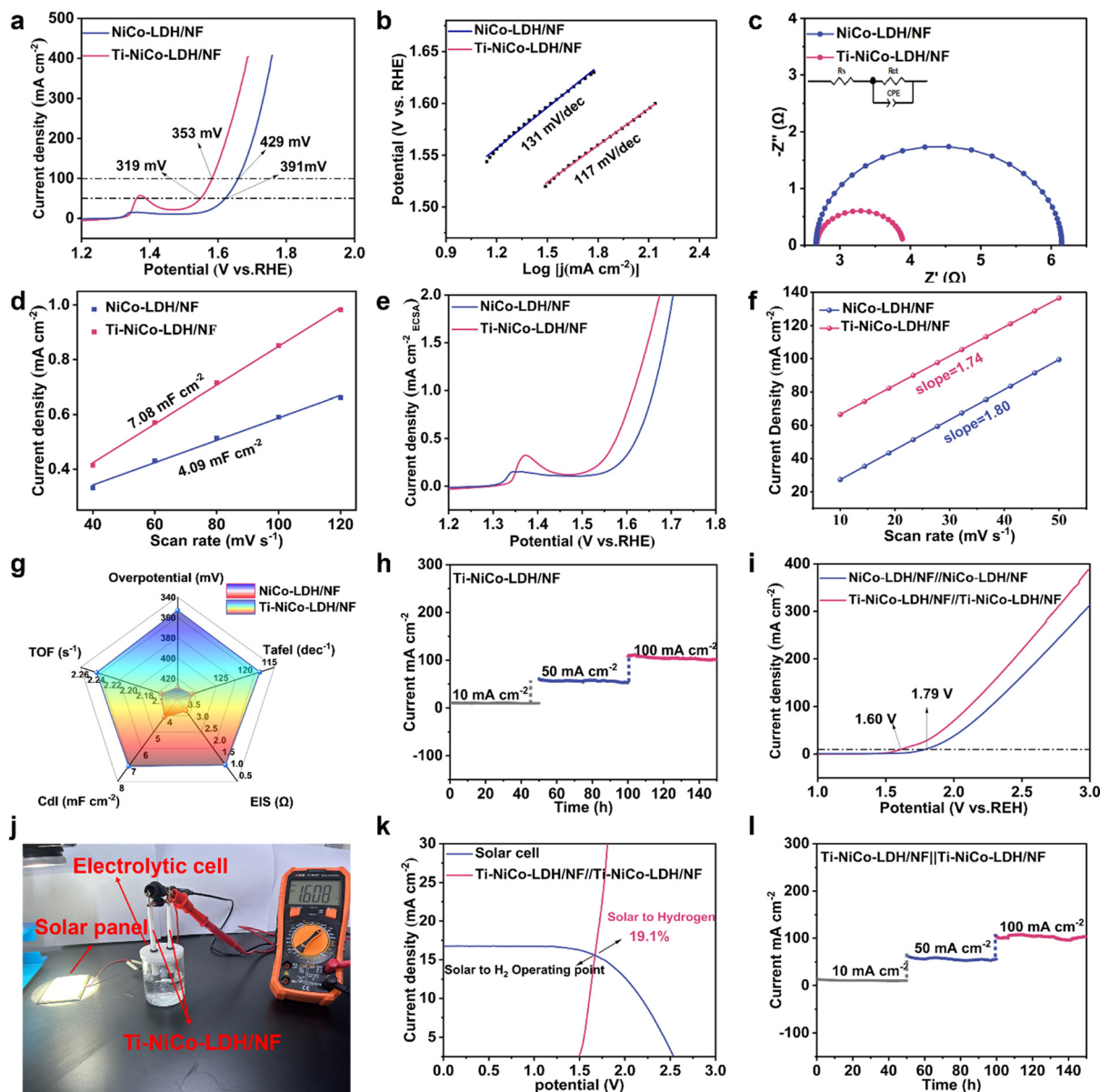
bonds, proves that the successful formation of M–O–Ti bonds leads to an increase in lattice oxygen.

The Raman spectrum of Ti-NiCo-LDH/NF showed two vibrational peaks at 459 and 520 cm^{-1}, which were attributed to the stretching vibration of M–O(H) and M–O. Besides, Ti-NiCo-LDH/NF showed higher full width at half maximum (FWHM) of M–O vibration modes compared with NiCo-LDH/NF, which was originated from the defective structure of Ti-NiCo-LDH/NF.[40] Besides, the presence of oxygen vacancies (O_V) was examined via electron spin resonance (ESR) spectroscopy (Fig. 2f). It was clearly observed that there is a stronger signal peak at $g = 2.003$, indicating the formation of more oxygen vacancies in Ti-NiCo-LDH/NF after Ti species doping. The atomic radius and coordination configuration of Ti atoms were different from those of Ni and Co atoms, which were inclined to cause lattice distortions and thus resulted in the oxygen vacancy-enriched feature.

2.2 Electrochemical performances of the catalysts

The electrochemical performance of NiCo-LDH/NF and Ti-NiCo-LDH/NF was tested in a conventional three-electrode test system in 1.0 M KOH solution. As shown in Fig. 3a, the linear scanning voltammetry (LSV) curves of Ti-NiCo-LDH/NF and other catalysts for the OER were obtained. Apparently, the Ti-NiCo-LDH/NF electrode exhibited the best OER activity with overpotentials of 319 and 353 mV at current densities of 50 and 100 mA cm^{-2}, respectively, which was superior to NiCo-LDH/NF and many recently reported NiCo-based catalysts (Table 1). This result suggested that the formation of M–O–Ti bonds by the reaction of $TiCl_4$ with NiCo-LDH/NF was essential for the enhancement of OER activity.

© 2025 The Author(s). Co-published by the Institute of Process Engineering, Chinese Academy of Sciences and the Royal Society of Chemistry

Ind. Chem. Mater., 2025, **3**, 342–352 | **345**

Fig. 3 Electrochemical OER performance of Ni-LDH/NF and Ti-NiCo-LDH/NF: (a) LSV curves corrected with iR compensation; (b) Tafel slopes; (c) impedance spectroscopy; (d) C_{dl} curves; (e) polarization curves after ECSA normalization; (f) turnover frequencies (TOFs); (g) radar chart showing Tafel slopes, EIS, C_{dl}, TOF, overpotential@j = 100 mA cm^{-2} of two samples; (h) chronoamperometry i–t tests; (i) LSV curves of Ti-NiCo-LDH/NF||Ti-NiCo-LDH/NF for overall water splitting in 1 M KOH; (j) an optical image of sunlight-driven water splitting; (k) STH; (l) chronoamperometry i–t tests.

Meanwhile, the reaction kinetics of catalysts were obtained *via* the Tafel slopes fitted by the LSV curves (Fig. 3b). The Tafel slope of the Ti-NiCo-LDH/NF catalyst was determined to be 117 mV dec^{-1}, which was lower than that of NiCo-LDH/NF (131 mV dec^{-1}), suggesting a much faster charge transfer kinetics.[33,41] Additionally, the charge transfer rate was further evaluated using electrochemical impedance spectroscopy (EIS) (Fig. 3c), and Ti-NiCo-LDH/NF exhibited a smaller charge transfer impedance with an R_{ct} value of 1.2 Ω, suggesting that the formation of the M–O–Ti bond lowered the electrical resistance and provided better electrical conductivity.[42,43]

To assess the electrochemical surface area (ECSA) of the electrocatalysts, the double layer capacitance C_{dl} (Fig. 3d) of

the two catalysts was obtained by analyzing the cyclic voltammetry (CV) curves collected in a non-faradaic region at different scanning rates.[44] Based on this, the ECSA of Ti-NiCo-LDH/NF was estimated to be 177 cm^{-2}, which was higher than that NiCo-LDH/NF (102.25 cm^{-2}). The larger ECSA of Ti-NiCo-LDH/NF was attributed to its spherical structure, and thus increased the reactive area. To further assess intrinsic activities, the activity areas were calculated through normalization ECSA (Fig. 3e), highlighting its superior intrinsic activity.

The turnover frequency (TOF) can be used as a reliable indicator to assess the intrinsic activity of the active sites of the electrocatalysts. Therefore, the TOF of the catalysts was

evaluated by using the oxidation peak current method at a current density of 100 mA cm^{-2} (Fig. 3f). The TOF value (2.24 s^{-1}) for Ti-NiCo-LDH/NF was slightly larger than that for NiCo-LDH/NF (2.16 s^{-1}) in both cases, indicating that the doping of titanium effectively increased the exposed active sites. Fig. 3g provides a clearer comparison between Ti-NiCo-LDH/NF and NiCo-LDH/NF concerning the Tafel slope, EIS, C_{dl}, TOF, and overpotential@j = 100 mA cm^{-2}. Moreover, the chronoamperometry (i–t) was used to assess the OER stability of Ti-NiCo-LDH/NF catalysts at 10, 50, and 100 mA cm^{-2}, respectively (Fig. 3h). The results showed that Ti-NiCo-LDH/NF maintained good stability after 150 h of continuous operation at different densities, demonstrating the excellent electrochemical durability of Ti-NiCo-LDH/NF.

To understand the performance of Ti-NiCo-LDH/NF in practical water decomposition, an alkaline electrolytic cell was assembled in 1.0 M KOH solution with Ti-NiCo-LDH/NF as the cathode and anode (Fig. 3i). The electrolytic cell required only a cell voltage of 1.6 V to drive a current density of 10 mA cm^{-2} and showed excellent stability for 150 h of cumulative operation at 10, 50, and 100 mA cm^{-2} (Fig. 3l). In addition, the overall water electrolysis performance of Ti-NiCo-LDH/NF was superior to many recently reported NiCo-based catalysts (Table 2).

Moreover, a solar-catalyzed water splitting system using a commercial silicon solar cell (a xenon lamp simulating sunlight as the light source) was assembled. As shown in Fig. 3j, the commercial solar cell was able to effectively drive water splitting with a voltage of 1.608 V. The above process produced a large number of bubbles on both electrodes, confirming its feasibility. The operating current density was 15.56 mA cm^{-2} at 1.23 V, and the solar to hydrogen (STH) efficiency was estimated to be 19.1% (Fig. 3k). High STH conversion efficiency holds promise for further development of Ti-NiCo-LDH/NF as a large-scale solar water separation electrocatalyst. In conclusion, the formation of M–O–Ti bonds improved the intrinsic activity and accelerated the electrocatalytic kinetics of Ti-NiCo-LDH/NF.

2.3 Mechanism analysis and density functional theory

To study the OER intermediates and understand the catalytic mechanism of Ti-NiCo-LDH/NF for the OER, *in situ* ATR-FTIR spectroscopy was employed in the potential range from an open circuit voltage (OCP) to 1.8 V. With an increasing potential, the energy band near 1230 cm^{-1} is the O–O stretching mode of surface-adsorbed superoxide (*OOH),[46–48] which indicated that both followed the traditional AEM mechanism (Fig. 4a and b).[49,50] Furthermore, after 1.5 V, the absorbance of Ti-NiCo-LDH/NF in this band increased noticeably, indicating that the oxygen-containing intermediate (*OOH) was enriched on the surface of electrocatalysts driven by applied bias. However, the absorbance of NiCo-LDH/NF did not change much with the potential increase. This suggested that the former showed the advantage of adsorbing oxygen-containing species under the potential, leading to a significant increase in their coverage and promoting the OER.[51]

To explore in depth the improvement of Ti-NiCo-LDH/NF activity and the effect of the M–O–Ti bond during the OER catalytic process, the Gibbs free energy pathway for the OER was calculated (Fig. 4e). In order to determine the real active sites, the rate-determining step (RDS) ΔG values of different model catalysts were calculated. The rate-determining step (RDS) ΔG values were in the order NiCo-LDH/NF (Co*) (1.969) > Ti-NiCo-LDH/NF (Co*) (1.792) > NiCo-LDH/NF (Ni*) (1.465) > Ti-NiCo-LDH/NF (Ni*) (1.322), suggesting that the OER active site for the above catalysts was more likely to take place at the Ni site instead of the Co site.

To investigate the interaction effect of M–O–Ti bonding on the reaction intermediates and metal adsorption sites, we calculated the d-band centers of Ni and Co in both catalysts. The Co site E_d values (Fig. 4c) for the two catalysts were −2.050 and −2.650 eV, respectively, and the Ni site E_d values (Fig. 4d) were −2.249 and −2.382 eV, respectively. According to the d-band center theory, the electrons in the antibonding orbitals were transferred to the bonding orbitals when the E_d was shifted to the E_f, which resulted in the enhancement of the intermediate product adsorption on the metal sites.[52] Conversely, when the d-band center was far away from the Fermi energy level, the adsorption effect was weaker, and it was difficult for the reactants to be activated and the subsequent reactions to occur. Medium adsorption strength favored the OER.[53] Therefore, the E_d values of Ni sites of both catalysts were in the middle range, which helped to regulate the adsorption and desorption of the reaction intermediates at Ni sites,[54] indicating that the OER process was more favorable to be carried out at Ni sites, which is in agreement with the above conclusion on the Gibbs free energy pathway. Moreover, the projected density of states (PDOS) of Ni 3d exhibited an upward shift (−2.382 eV) of the d-band center (−2.249 eV) of Ti-NiCo-LDH/NF as compared to NiCo LDH/NF.

Table 2 Comparison of OER performance and overall water splitting performance of NiCo-based catalysts

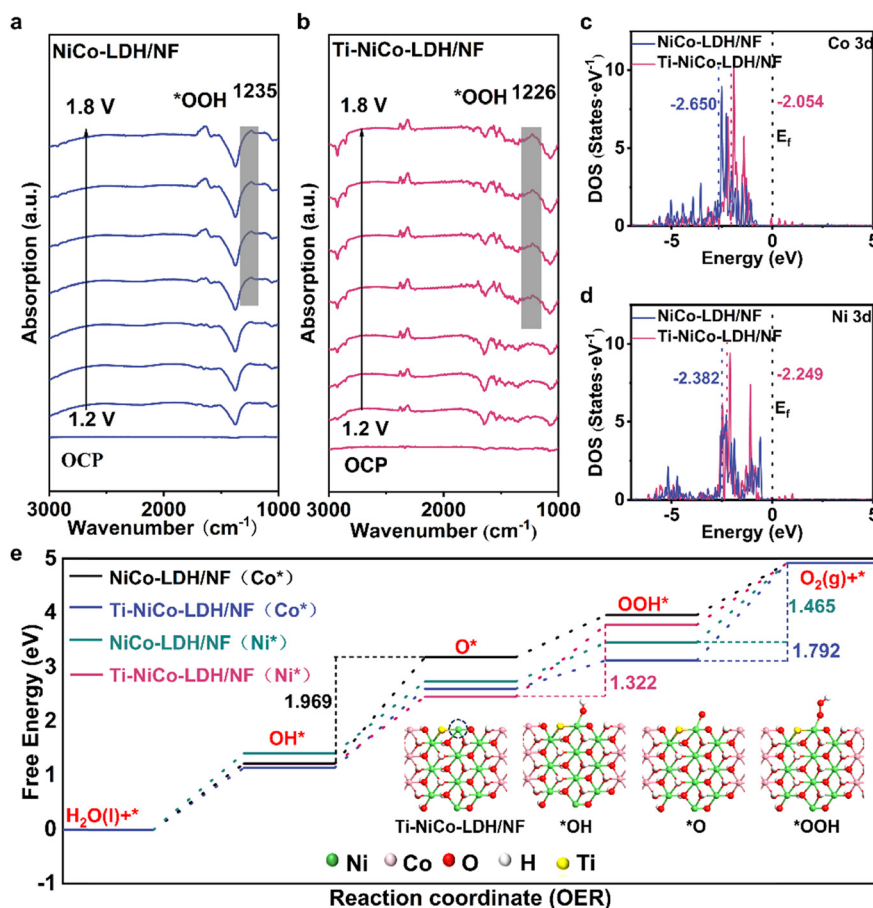| Catalysts	Overpotential (mV@50 mA cm^{-2})	Overpotential (mV@100 mA cm^{-2})	Voltage (V@10 mA cm^{-2})	Ref.
NiCoMo-LDH	290	350	1.62	13
Mo-NiCo LDHs/NF	330	360	1.67	21
Cu$_x$O@NiCoS-1/CF	351	430	1.65	33
3D Mo-NiCoP/NF	324	344	1.78	43
NiCoCe-LDH/RNF	299	490	—	45
NiCo-LDH/NF	391	429	1.79	This work
Ti-NiCo-LDH/NF	319	353	1.60	This work

© 2025 The Author(s). Co-published by the Institute of Process Engineering, Chinese Academy of Sciences and the Royal Society of Chemistry

Ind. Chem. Mater., 2025, **3**, 342–352 | 347

Fig. 4 *In situ* spectroscopic characterization: (a) NiCo-LDH/NF; (b) Ti-NiCo-LDH/NF; (c and d) the calculated DOS of NiCo-LDH/NF and Ti-NiCo-LDH/NF; (e) the OER free energy diagram for AEM steps and optimized intermediate geometry for Ni sites of Ti-NiCo-LDH/NF (inset).

This upward shift enhanced the adsorption strength of oxygen-containing intermediates (*e.g.*, *OOH) on the nickel active site. It was shown that the introduction of Ti can change the electronic structure of Ni, enhance the adsorption of oxygenated intermediates in the OER process, as well as the speed of electron transfer, and reduce the energy required to lower the RDS from 1.465 to 1.322 eV, thus promoting the OER reaction kinetics.[55–58] Therefore, DFT calculations demonstrated that Ti doping optimized the electronic structure of NiCo-LDH, lowered the reaction energy barriers, and promoted the increase of OER activity, which was in good agreement with the experimental analysis.

3 Conclusions

In conclusion, we reported a simple strategy for rapid modification of self-supported NiCo-LDH/NF with titanium tetrachloride at room temperature and investigated the catalytic mechanism of Ti-NiCo-LDH/NF for the OER process. Ti-NiCo-LDH/NF exhibited excellent OER activity in alkaline electrolytes with overpotentials of 319 and 353 mV at current densities of 50 and 100 mA cm^{-2}, respectively, and showed excellent stability. Moreover, only 1.60 V was required to drive water splitting. The experiment result and density functional

theory (DFT) calculations corroborated that the formation of M–O–Ti (M = Ni, Co) bonds by the reaction between TiCl$_4$ and NiCo-LDH optimized the electronic structure of Ni, thus facilitating the adsorption and resolution of the reaction intermediates. The introduction of Ti made lattice distortions and generated more oxygen vacancies, which leads to more active sites. The introduction of Ti improved the hydrophilicity of NiCo-LDH/NF, which was favorable for electrolyte diffusion as well as gas departure. Therefore, the work provides a new strategy for the rapid modification of self-supporting hydrotalcite to enhance the OER activity.

4 Experimental section

4.1 Materials and synthesis of NiCo-LDH/NF and Ti-NiCo-LDH/NF

Nickel nitrate hexahydrate (Ni(NO$_3$)·6H$_2$O), cobalt nitrate hexahydrate (Co(NO$_3$)$_2$·6H$_2$O), ammonium fluoride (NH$_4$F), urea (CON$_2$H$_4$), and silicon tetrachloride (TiCl$_4$) were purchased from McLean Corporation, and all reagents are of analytical grade and all chemicals are used directly as received. In the typical synthesis process, Ni(NO$_3$)·6H$_2$O (1.5 mmol), Co(NO$_3$)$_2$·6H$_2$O (0.75 mmol), NH$_4$F (6 mmol), and urea (12 mmol) were dissolved in 35 mL of deionized water

and stirred for 30 min to form the mixture solution. Subsequently, the cleaned commercial nickel foam (NF) (2 × 1 cm^2) was immersed in the above solution in a 50 mL Teflon-lined autoclave and reacted at 95 °C for 10 h. Finally, NiCo-LDH/NF was obtained by subsequent washing with deionized water and anhydrous ethanol and drying.

For the fabrication of Ti-NiCo-LDH/NF, the obtained NiCo-LDH/NF was placed into 2 mL of titanium tetrachloride solution (99.5%) and impregnated for 30 s. After that, the above product was taken out and rinsed with deionized water and dried in vacuum to obtain Ti-NiCo-LDH/NF.

4.2 Catalyst characterization

The chemical composition and phase structure were characterized by X-ray diffraction (XRD) using a D8 Advance instrument from Bruker with Cu Kα as the radiation source (λ = 1.541 nm). The scan range was set to 3–90° (2θ) and the scan rate was 5 °C min^{-1}. The microstructure and morphology were characterized using a scanning electron microscope (SEM, Hitachi S4800) and transmission electron microscope (TEM FEI Tecnai G2 F20) equipped with an energy-dispersive X-ray (EDX) spectrometer. X-ray photoelectron spectroscopy (XPS) was performed with a Thermo ESCALAB 250XI, Thermo Fisher Scientific. Electron spin resonance (ESR) was performed on an A300-10/12 spectrometer from Bruker, Germany. FTIR spectra were obtained using a Bruker Vertex 70. Raman spectroscopy was performed using a Renishaw inVia from Renishaw UK (the laser wavelength is 514 nm). *In situ* ATR-FTIR measurement was carried out using an FT-IR spectrometer TENSOR37 *via* a three-electrode setup with Ti-NiCo-LDH/NF or NiCo-LDH/NF as the working electrode, Pt as the counter electrode and Hg/HgO as the reference electrode.

4.3 Electrochemical performance test

All electrochemical measurements were performed in a standard three-electrode setup on an electrochemical workstation (CHI760E, CH Instruments Inc.) in a 1 M KOH electrolyte, using a graphite rod and Hg/HgO as counter and reference electrodes, respectively, and the loaded NF as the working electrode. All polarization curves were recorded with 95% iR compensation and the potential was referenced to the reversible hydrogen electrode (RHE): E(RHE) = E(Hg/HgO) + 0.098 + 0.059 pH.

4.4 Theoretical calculations

Density functional theory (DFT) calculations were carried out to clarify the adsorption free energy of various oxygenated species during the OER process. The valence–core electron interactions were treated by projector augmented wave (PAW) potentials and the electron exchange–correlation interactions were described by the generalized gradient approximation (GGA) with the Perdew–Burke–Ernzerhof (PBE). Considering the long-range interaction between molecules/intermediates and the

surface, van der Waals interactions were considered using DFT-D3 correlation. To avoid effects coming from other slabs, a vacuum of 25 A was added along the z direction. The convergence criterion of residual force and energy in the geometry relaxation was set to 0.001 eV $Å^{-1}$ and 10^{-4} eV, respectively (E_{DIFFG} = −0.001; E_{DIFF} = 1 × 10^{-4}). The energy cutoff for the plane wave-basis was set to 550 eV (E_{NCUT} = 550). The k points were sampled with 4 × 4 × 1 by the Monkhorst–Pack method. Moreover, the k points were set as 8 × 8 × 1 for the electronic static calculation (density of states, electron localization function, and bonding analysis), and meanwhile, the energy cut-off of the plane wave was increased to 750 eV. Free energies of each reaction step were calculated by the following formula: $G = E_{DFT} + E_{ZPE} - T\Delta S$, where E_{DFT} is the DFT calculated energy, and E_{ZPE} and $T\Delta S$ are calculated by DFT vibration frequency calculations. To consider the effect of an applied electric potential on the electrode reaction, a value of $-n_eU$ was added to calculate the free energy of each step, where n is the number of electrons involved in the reaction and U is the applied bias.

Data availability

All data included in this article are available upon request by contacting the corresponding author.

Conflicts of interest

The authors declare that they have no known competing financial interests or personal relationships that could have appeared to influence the work reported in this paper.

Acknowledgements

References

1 S. A. Mirshokraee, M. Muhyuddin, J. Orsilli, E. Berretti, L. Capozzoli, A. Lavacchi, C. Lo Vecchio, V. Baglio, A. Galli, A. Zaffora, F. Di Franco, M. Santamaria, L. Olivi, S. Pollastri and C. Santoro, Mono-, bi- and tri-metallic platinum group metal-free electrocatalysts for hydrogen evolution reaction following a facile synthetic route, *Ind. Chem. Mater.*, 2023, **1**, 343–359.

2 X. Yu, Y. Li, C. Pei, Y. Lu, J. K. Kim, H. S. Park and H. Pang, Interfacial design of $Ti_3C_2T_x$ MXene/Graphene heterostructures boosted Ru nanoclusters with high activity toward hydrogen evolution reaction, *Adv. Sci.*, 2024, **11**, 2310013.

3 J. Ding, D. Zhang, A. Riaz, H. Gu, J. Zheyan Soo, P. Reddy Narangari, C. Jagadish, H. Hoe Tan and S. Karuturi, Scalable amorphous NiFe(OH)x/Fe/Graphene bifunctional electrocatalyst via solution-corrosion for water splitting, *CCS Chem.*, 2024, **6**, 2692–2703.

© 2025 The Author(s). Co-published by the Institute of Process Engineering, Chinese Academy of Sciences and the Royal Society of Chemistry

Ind. Chem. Mater., 2025, **3**, 342–352 | **349**

4 Y. Pan, Z. Wang, K. Wang, Q. Ye, B. Shen, F. Yang and Y. Cheng, Dual doping of B and Fe activated Lattice oxygen participation for enhanced oxygen evolution reaction activity in alkaline freshwater and seawater, *Adv. Funct. Mater.*, 2024, **34**, 202402264.

5 F. Wu, F. Tian, M. Li, S. Geng, L. Qiu, L. He, L. Li, Z. Chen, Y. Yu, W. Yang and Y. Hou, Engineering lattice oxygen regeneration of NiFe layered double hydroxide enhances oxygen evolution catalysis durability, *Angew. Chem., Int. Ed.*, 2024, **64**, e202413250.

6 J. Cao, D. Zhang, B. Ren, P. Song and W. Xu, Mn incorporated RuO$_2$ nanocrystals as an efficient and stable bifunctional electrocatalyst for oxygen evolution reaction and hydrogen evolution reaction in acid and alkaline, *Chin. Chem. Lett.*, 2024, **35**, 109863.

7 T. Zhang, J. Jiang, W. Sun, S. Gong, X. Liu, Y. Tian and D. Wang, Spatial configuration of Fe-Co dual-sites boosting catalytic intermediates coupling toward oxygen evolution reaction, *Proc. Natl. Acad. Sci. U. S. A.*, 2024, **121**, 2317247121.

8 H. He, P. Kou, Z. Zhang, D. Wang, R. Zheng, H. Sun, Y. Liu and Z. Wang, Coupling high entropy oxide with hollow carbon spheres by rapid microwave solvothermal strategy for boosting oxygen evolution reaction, *J. Colloid Interface Sci.*, 2024, **653**, 179–188.

9 B. Zhang, X. Zhang, Y. Wei, L. Xia, C. Pi, H. Song, Y. Zheng, B. Gao, J. Fu and P. K. Chu, General synthesis of NiCo alloy nanochain arrays with thin oxide coating: a highly efficient bifunctional electrocatalyst for overall water splitting, *J. Alloys Compd.*, 2019, **797**, 1216–1223.

10 X. Yu, Z. Pan, C. Pei, L. Lin, Y. Lu, H. S. Park and H. Pang, Core-shell heterostructure by coupling layered ReS$_2$ with Co$_9$S$_8$ nanocubes for boosted oxygen evolution reaction, *Chin. Chem. Lett.*, 2024, **35**, 108484.

11 W. He, R. Zhang, H. Liu, Q. Hao, Y. Li, X. Zheng, C. Liu, J. Zhang and H. L. Xin, Atomically dispersed silver atoms embedded in NiCo layer double hydroxide boost oxygen evolution reaction, *Small*, 2023, **19**, 202301610.

12 H. Wang, N. Jiang, B. Huang, Q. Yu and L. Guan, Surface amorphization and functionalization of a NiFeOOH electrocatalyst for a robust seawater electrolyzer, *EES Catal.*, 2024, **2**, 1092–1099.

13 S. M. N. Jeghan, N. Kim and G. Lee, Mo-incorporated three-dimensional hierarchical ternary nickel-cobalt-molybdenum layer double hydroxide for high-efficiency water splitting, *Int. J. Hydrogen Energy*, 2021, **46**, 22463–22477.

14 X. Zhang, J. Fan, X. Lu, Z. Han, C. Cazorla, L. Hu, T. Wu and D. Chu, Bridging NiCo layered double hydroxides and Ni$_3$S$_2$ for bifunctional electrocatalysts: The role of vertical graphene, *Chem. Eng. J.*, 2021, **415**, 129048.

15 J. Yu, Y. Zhang, N. Zhang, J. Li, H. Sun, X. Gu, C. Ye, T. Liu and Y. Du, The interface engineering strategy assists the 3D core-shell structure Co$_3$S$_4$/CuS@NiFe LDH nanocoral spheres to achieve significant overall water splitting, *Chin. Chem. Lett.*, 2025, DOI: 10.1016/j.cclet.2025.110830.

16 W. Zhao, H. Xu, H. Luan, N. Chen, P. Gong, K. Yao, Y. Shen and Y. Shao, NiFe layered double hydroxides grown on a corrosion-cell cathode for oxygen evolution electrocatalysis, *Adv. Energy Mater.*, 2021, **12**, 202102372.

17 X. Han, N. Li, J. S. Baik, P. Xiong, Y. Kang, Q. Dou, Q. Liu, J. Y. Lee, C. S. Kim and H. S. Park, Sulfur mismatch substitution in layered double hydroxides as efficient oxygen electrocatalysts for flexible Zinc-Air batteries, *Adv. Funct. Mater.*, 2023, **33**, 2212233.

18 H. Liao, G. Ni, P. Tan, K. Liu, X. Liu, H. Liu, K. Chen, X. Zheng, M. Liu and J. Pan, Oxyanion engineering suppressed iron segregation in Nickel-Iron catalysts toward stable water oxidation, *Adv. Mater.*, 2023, **35**, 2300347.

19 W. Wang, Y. Liu and S. Chen, Use of NiFe layered double hydroxide as electrocatalyst in oxygen evolution reaction: Catalytic mechanisms, electrode design, and durability, *Acta Phys.-Chim. Sin.*, 2024, **40**, 2303059.

20 J. Abed, S. Ahmadi, L. Laverdure, A. Abdellah, C. P. O'Brien, K. Cole, P. Sobrinho, D. Sinton, D. Higgins, N. J. Mosey, S. J. Thorpe and E. H. Sargent, In situ formation of nano Ni-Co oxyhydroxide enables water oxidation electrocatalysts durable at high current densities, *Adv. Mater.*, 2021, **33**, 202103812.

21 K. Chen, Y.-H. Cao, S. Yadav, G.-C. Kim, Z. Han, W. Wang, W.-J. Zhang, V. Dao and I.-H. Lee, Electronic structure reconfiguration of nickel-cobalt layered double hydroxide nanoflakes via engineered heteroatom and oxygen-vacancies defect for efficient electrochemical water splitting, *Chem. Eng. J.*, 2023, **463**, 142396.

22 P. Zhou, Y. Wang, C. Xie, C. Chen, H. Liu, R. Chen, J. Huo and S. Wang, Acid-etched layered double hydroxides with rich defects for enhancing the oxygen evolution reaction, *Chem. Commun.*, 2017, **53**, 11778–11781.

23 S. Du, Z. Ren, X. Wang, J. Wu, H. Meng and H. Fu, Controlled atmosphere corrosion engineering toward Inhomogeneous NiFe-LDH for energetic oxygen evolution, *ACS Nano*, 2022, **16**, 7794–7803.

24 J. Yan, L. Chen and X. Liang, Co$_9$S$_8$ nanowires@NiCo LDH nanosheets arrays on nickel foams towards efficient overall water splitting, *Sci. Bull.*, 2019, **64**, 158–165.

25 Y. Liao, R. He, W. Pan, Y. Li, Y. Wang, J. Li and Y. Li, Lattice distortion induced Ce-doped NiFe-LDH for efficient oxygen evolution, *Chem. Eng. J.*, 2023, **464**, 142669.

26 T. Wang, H. Wu, C. Feng, L. Zhang and J. Zhang, MoP@NiCo-LDH on nickel foam as bifunctional electrocatalyst for high efficiency water and urea-water electrolysis, *J. Mater. Chem. A*, 2020, **8**, 18106–18116.

27 S. Li, L. Wang, Y. Li, L. Zhang, A. Wang, N. Xiao, Y. Gao, N. Li, W. Song, L. Ge and J. Liu, Novel photocatalyst incorporating Ni-Co layered double hydroxides with P-doped CdS for enhancing photocatalytic activity towards hydrogen evolution, *Appl. Catal., B*, 2019, **254**, 145–155.

28 H. Yang, Z. Zhou, H. Yu, H. Wen, R. Yang, S. Peng, M. Sun and L. Yu, Alkali treatment of layered double hydroxide nanosheets as highly efficient bifunctional electrocatalysts for overall water splitting, *J. Colloid Interface Sci.*, 2023, **636**, 11–20.

29 Q. Xu, P. Wang, L. Wan, Z. Xu, M. Z. Sultana and B. Wang, Superhydrophilic/superaerophobic hierarchical NiP_2@MoO_2/Co(Ni)MoO_4 core-shell array electrocatalysts for efficient hydrogen production at large current densities, *ACS Appl. Mater. Interfaces*, 2022, **14**, 19448–19458.

30 C.-P. Wang, H. Sun, G. Bian, J.-X. Wang, X. Pang, G. Wang, J. Zhu and X.-H. Bu, Electrostatically connected nanoarchitected electrocatalytic films for boosted water splitting, *Nano Res.*, 2023, **17**, 1114–1122.

31 M. Li, H. Li, X. Jiang, M. Jiang, X. Zhan, G. Fu, J.-M. Lee and Y. Tang, Gd-induced electronic structure engineering of a NiFe-layered double hydroxide for efficient oxygen evolution, *J. Mater. Chem. A*, 2021, **9**, 2999–3006.

32 B. Chen, Z. Zhang, S. Kim, M. Baek, D. Kim and K. Yong, A biomimetic nanoleaf electrocatalyst for robust oxygen evolution reaction, *Appl. Catal., B*, 2019, **259**, 118017.

33 C. Song, J. Yang, C. Ayappan, H. Yang, R. Xing and S. Liu, In situ construction of heterostructured CuxO@NiCoS nanoarrays for alkaline overall water splitting, *Sustainable Energy Fuels*, 2024, **8**, 302–309.

34 D. Gao, J. Guo, H. He, P. Xiao and Y. Zhang, Geometric and electronic modulation of fcc NiCo alloy by Group-VI B metal doping to accelerate hydrogen evolution reaction in acidic and alkaline media, *Chem. Eng. J.*, 2022, **430**, 133110.

35 Y. Feng, X. Wang, J. Huang, P. Dong, J. Ji, J. Li, L. Cao, L. Feng, P. Jin and C. Wang, Decorating CoNi layered double hydroxides nanosheet arrays with fullerene quantum dot anchored on Ni foam for efficient electrocatalytic water splitting and urea electrolysis, *Chem. Eng. J.*, 2020, **390**, 124525.

36 K. Zheng, J. Ren, X. Li, G. Li, L. Jiao and C. Xu, Engineering crystalline CoMP-decorated (M = Mn, Fe, Ni, Cu, Zn) amorphous CoM LDH for high-rate alkaline water splitting, *Chem. Eng. J.*, 2022, **441**, 136031.

37 X. Xia, S. Wang, D. Liu, F. Wang, X. Zhang, H. Zhang, X. Yu, Z. Pang, G. Li, C. Chen, Y. Zhao, L. Ji, Q. Xu, X. Zou and X. Lu, Electronic modulation in Cu doped NiCo LDH/NiCo heterostructure for highly efficient overall water splitting, *Small*, 2024, **20**, 202311182.

38 S. Zheng, Y. Zhang, Q. Chen, X. Fu, Q. Huang, Z. Bin, H. Dong and C. Li, Exploring the synergistic benefits of insoluble dietary fiber and bound phenolics: Unveiling the role of bound phenolics in enhancing bioactivities of insoluble dietary fiber, *Trends Food Sci. Technol.*, 2024, **149**, 104554.

39 J. He, X. Zhou, P. Xu and J. Sun, Promoting electrocatalytic water oxidation through tungsten-modulated oxygen vacancies on hierarchical FeNi-layered double hydroxide, *Nano Energy*, 2021, **80**, 105540.

40 S. Zhou, H. He, J. Li, Z. Ye, Z. Liu, J. Shi, Y. Hu and W. Cai, Regulating the band structure of Ni active sites in few-layered Nife-LDH by in situ adsorbed borate for ampere-level oxygen evolution, *Adv. Funct. Mater.*, 2023, **34**, 2313770.

41 Z. Q. Ge, J. Li, H. J. Zhang, C. Liu, G. Che and Z. Q. Liu, p-d Orbitals Coupling Heterosites of Ni_2P/NiFe-LDH Interface Enable O-H Cleavage for Water Splitting, *Adv. Funct. Mater.*, 2024, **202411024**, DOI: **10.1002/adfm.202411024**.

42 J.-W. Zhao, Z.-X. Shi, C.-F. Li, L.-F. Gu and G.-R. Li, Boosting the electrocatalytic performance of NiFe layered double hydroxides for the oxygen evolution reaction by exposing the highly active edge plane (012), *Chem. Sci.*, 2021, **12**, 650–659.

43 C. Sun, Y. He, N. S. Alharbi, S. Yang and C. Chen, Three-dimensional ordered macroporous molybdenum doped NiCoP honeycomb electrode for two-step water electrolysis, *J. Colloid Interface Sci.*, 2023, **642**, 13–22.

44 L. Tan, H. Wang, C. Qi, X. Peng, X. Pan, X. Wu, Z. Wang, L. Ye, Q. Xiao, W. Luo, H. Gao, W. Hou, X. Li and T. Zhan, Regulating Pt electronic properties on NiFe layered double hydroxide interface for highly efficient alkaline water splitting, *Appl. Catal., B*, 2024, **342**, 123352.

45 R. Qi, Z. Zhong, Y. Jia, F. Chen, Y. Yang, X. Zheng, Q. Li, Q. Ye and H. Du, Ce-doped NiCo-layered double hydroxide based self-supporting tremella-shaped nanoflower heterostructure as efficient electrocatalyst for the oxygen evolution reaction, *J. Environ. Chem. Eng.*, 2024, **12**, 114376.

46 S. Ji, Y. Mou, H. Liu, X. Lu, Y. Zhang, C. Guo, K. Sun, D. Liu, J. H. Horton, C. Wang, Y. Wang and Z. Li, Manipulating the electronic properties of an Fe single atom catalyst via secondary coordination sphere engineering to provide enhanced oxygen electrocatalytic activity in Zinc-Air batteries, *Adv. Mater.*, 2024, **36**, 2410121.

47 Y. Hu, Y. Zheng, J. Jin, Y. Wang, Y. Peng, J. Yin, W. Shen, Y. Hou, L. Zhu, L. An, M. Lu, P. Xi and C.-H. Yan, Understanding the sulphur-oxygen exchange process of metal sulphides prior to oxygen evolution reaction, *Nat. Commun.*, 2023, **14**, 1949.

48 S. Nayak, I. J. McPherson and K. A. Vincent, Adsorbed intermediates in oxygen reduction on platinum nanoparticles observed by in situ iR spectroscopy, *Angew. Chem., Int. Ed.*, 2018, **57**, 12855–12858.

49 J. Xu, H. Jin, T. Lu, J. Li, Y. Liu, K. Davey, Y. Zheng and S.-Z. Qiao, IrOx·nH_2O with lattice water-assisted oxygen exchange for high-performance proton exchange membrane water electrolyzers, *Sci. Adv.*, 2023, **9**, eadh1718.

50 Y. Yao, S. Hu, W. Chen, Z.-Q. Huang, W. Wei, T. Yao, R. Liu, K. Zang, X. Wang, G. Wu, W. Yuan, T. Yuan, B. Zhu, W. Liu, Z. Li, D. He, Z. Xue, Y. Wang, X. Zheng, J. Dong, C.-R. Chang, Y. Chen, X. Hong, J. Luo, S. Wei, W.-X. Li, P. Strasser, Y. Wu and Y. Li, Engineering the electronic structure of single atom Ru sites via compressive strain boosts acidic water oxidation electrocatalysis, *Nat. Catal.*, 2019, **2**, 304–313.

51 L. Guo, Z. Zhang, Z. Mu, P. Da, L. An, W. Shen, Y. Hou, P. Xi and C. H. Yan, Ceria-optimized oxygen-species exchange in hierarchical bimetallic hydroxide for electrocatalytic water oxidation, *Adv. Mater.*, 2024, **36**, 202406682.

52 X. Wang, W. Pi, S. Hu, H. Bao, N. Yao and W. Luo, Boosting oxygen evolution reaction performance on NiFe-Based catalysts through d-orbital hybridization, *Nano-Micro Lett.*, 2025, **17**, 11.

© 2025 The Author(s). Co-published by the Institute of Process Engineering, Chinese Academy of Sciences and the Royal Society of Chemistry

Ind. Chem. Mater., 2025, **3**, 342–352 | **351**

53 G. Zhou, G. Liu, X. Liu, Q. Yu, H. Mao, Z. Xiao and L. Wang, 1D/3D heterogeneous assembling body as trifunctional electrocatalysts enabling Zinc-Air battery and self-powered overall water splitting, *Adv. Funct. Mater.*, 2021, **32**, 202107608.

54 J. Qu, Y. Dong, T. Zhang, C. Zhao, L. Wei and X. Guan, Impact of bimetallic synergies on Mo-doping NiFeOOH: Insights into enhanced OER activity and reconstructed electronic structure, *Front. Energy*, 2024, **18**, 850–862.

55 S. Sun, X. Zhou, B. Cong, W. Hong and G. Chen, Tailoring the d-band centers endows (NixFe1–x)2P nanosheets with efficient oxygen evolution catalysis, *ACS Catal.*, 2020, **10**, 9086–9097.

56 W. Cheng, S. Xi, Z.-P. Wu, D. Luan and X. W. Lou, In situ activation of Br-confined Ni-based metal-organic framework hollow prisms toward efficient electrochemical oxygen evolution, *Sci. Adv.*, 2021, **7**, abk0919.

57 Z. Xiao, W. Zhou, B. Yang, C. Liao, Q. Kang, G. Chen, M. Liu, X. Liu, R. Ma and N. Zhang, Tuned d-band states over lanthanum doped nickel oxide for efficient oxygen evolution reaction, *Nano Mater. Sci.*, 2023, **5**, 228–236.

58 Y. Hu, T. Shen, Z. Wu, Z. Song, X. Sun, S. Hu and Y. F. Song, Coordination stabilization of Fe by porphyrin-intercalated NiFe-LDH under industrial-level alkaline conditions for long-term electrocatalytic water oxidation, *Adv. Funct. Mater.*, 2024, **35**, 2413533.